




ORIGINAL ARTICLE

OPEN

Loss of KDM6B epigenetically confers resistance to lipotoxicity in nonalcoholic fatty liver disease–related HCC

Megumi Hatano¹ | Yoshimitsu Akiyama¹  | Shu Shimada¹  | Kohei Yagi^{1,2} | Keiichi Akahoshi² | Michiko Itoh³ | Minoru Tanabe² | Yoshihiro Ogawa⁴ | Shinji Tanaka^{1,2} 

¹Department of Molecular Oncology, Graduate School of Medicine, Tokyo Medical and Dental University, Tokyo, Japan

²Department of Hepato-Biliary-Pancreatic Surgery, Graduate School of Medicine, Tokyo Medical and Dental University, Tokyo, Japan

³Kanagawa Institute of Industrial Science and Technology, Kanagawa, Japan

⁴Department of Medicine and Bioregulatory Science, Graduate School of Medical Sciences, Kyushu University, Fukuoka, Japan

Correspondence

Yoshimitsu Akiyama, Department of Molecular Oncology, Graduate School of Medicine, Tokyo Medical and Dental University, 1-5-45 Yushima, Bunkyo-Ku, Tokyo 113-8519, Japan. Email: yakiyama.monc@tmd.ac.jp

Shinji Tanaka, Department of Molecular Oncology, Graduate School of Medicine, Tokyo Medical and Dental University, 1-5-45 Yushima, Bunkyo-Ku, Tokyo 113-8519, Japan. Email: tanaka.monc@tmd.ac.jp

Abstract

Background: NAFLD caused by abnormalities in hepatic lipid metabolism is associated with an increased risk of developing HCC. The molecular mechanisms underlying the progression of NAFLD-related HCC are not fully understood. We investigated the molecular mechanism and role of KDM6B downregulation in NAFLD-related HCC after the *KDM6B* gene was identified using microarray analysis as commonly downregulated in mouse NAFLD-related HCC and human nonhepatitis B and nonhepatitis C viral-HCC.

Methods: The 5-hydroxymethylcytosine levels of KDM6B in HCC cells were determined using glycosylated hydroxymethyl-sensitive PCR. Microarray and chromatin immunoprecipitation analyses using *KDM6B*-knockout (KO) cells were used to identify KDM6B target genes. Lipotoxicity was assessed using a palmitate-treated cell proliferation assay. Immunohistochemistry was used to evaluate KDM6B expression in human HCC tissues.

Results: KDM6B expression levels in HCC cells correlated with the 5-hydroxymethylcytosine levels in the *KDM6B* gene body region. Gene set enrichment analysis revealed that the lipid metabolism pathway was suppressed in *KDM6B*-KO cells. *KDM6B*-KO cells acquired resistance to lipotoxicity ($p < 0.01$) and downregulated the expression of *G0S2*, an adipose triglyceride lipase/patatin like phospholipase domain containing 2 (ATGL/PNPLA2) inhibitor, through increased histone H3 lysine-27 trimethylation levels. *G0S2* knockdown in *KDM6B*-expressed HCC cells conferred lipotoxicity resistance, whereas ATGL/PNPLA2 inhibition in the *KDM6B*-KO cells reduced these effects. Immunohistochemistry revealed that KDM6B expression was decreased in human NAFLD-related HCC tissues ($p < 0.001$), which was

Abbreviations: ATGL, adipose triglyceride lipase; ChIP, chromatin immunoprecipitation; G0S2, G0/G1 switch 2; H3K27 me3, histone H3 lysine-27 trimethylation; 5hmC, 5-hydroxymethylcytosine; KO, knockout; MC4R, melanocortin type 4 receptor; NBNC, nonhepatitis B and nonhepatitis C viral; PNPLA2, patatin like phospholipase domain containing 2; siRNA, small interfering RNA; TCGA, The Cancer Genome Atlas; WT, wild-type.

Supplemental Digital Content is available for this article. Direct URL citations are provided in the HTML and PDF versions of this article on the journal's website, www.hepcommjournal.com.

This is an open access article distributed under the terms of the Creative Commons Attribution-Non Commercial-No Derivatives License 4.0 (CCBY-NC-ND), where it is permissible to download and share the work provided it is properly cited. The work cannot be changed in any way or used commercially without permission from the journal.

Copyright © 2023 The Author(s). Published by Wolters Kluwer Health, Inc. on behalf of the American Association for the Study of Liver Diseases.

significantly associated with decreased *G0S2* expression ($p = 0.032$).

Conclusions: KDM6B-disrupted HCC acquires resistance to lipotoxicity via ATGL/PNPLA2 activation caused by epigenetic downregulation of *G0S2* expression. Reduced KDM6B and *G0S2* expression levels are common in NAFLD-related HCC. Targeting the KDM6B-*G0S2*-ATGL/PNPLA2 pathway may be a useful therapeutic strategy for NAFLD-related HCC.

INTRODUCTION

NAFLD, which is caused by hepatic lipid metabolism abnormalities, is associated with metabolic risk factors, such as obesity, dyslipidemia, hypertension, and diabetes^[1]. The prevalence of NAFLD is increasing with the rise in the obese population worldwide^[2]. Although NAFLD has a better prognosis than alcohol-associated fatty liver disease, some cases have been found to progress to NASH with fibrosis, which can lead to the development of HCC^[3,4]. HCC is the world's fourth most common cancer^[2]. In recent years, the increase in the number of HBV surface antigen-negative and HCV antibody-negative HCC (NBNC-HCC) cases has exceeded 30%^[1]. The rise in NBNC-HCC is thought to be due to an increase in the number of patients with NAFLD^[5]. Nagaoki et al^[6] reported that 14.9% of HCC cases are associated with NASH/NAFLD in patients with NBNC-HCC.

Studies on NASH-related HCC have been conducted using high-fat diet-fed and genetically modified mice^[7]. Our group previously reported a mouse model with a knockout (KO) of the melanocortin type 4 receptor (*MC4R*^{-/-}), which develops NASH-like lesions and multiple liver tumors when fed a high-fat diet, similar to patients with obesity^[8]. In addition, the HCC gene expression pattern from *MC4R*^{-/-} mice closely resembles that of human HCC with metabolic risk factors^[9], suggesting that the *MC4R*^{-/-} mice are a useful model for HCC with metabolic syndrome.

In hepatic cells, epigenetic mechanisms, including DNA methylation and histone modification, are crucial for regulating lipid metabolism, insulin resistance, oxidative stress response, and inflammation^[10,11]. NAFLD has recently been linked to dynamic changes in 5-hydroxymethylcytosine (5hmC) patterns throughout the genome^[12]. Evidence suggests that histone modification changes cause transcriptional dysregulation of lipogenic-related and glycolytic-related genes involved in the development of NAFLD and NASH^[12-14]. However, the molecular mechanism of NAFLD-related HCC progression via epigenetic dysregulation is not fully understood.

To investigate the role of epigenetic factors in NAFLD-related HCC in this study, we first reanalyzed microarray data from mouse *MC4R*^{-/-}-HCC and human NBNC-HCC^[9]. *KDM6B* (lysine K-specific demethylase 6B, also known as JMJD3) was found to be a commonly

downregulated gene in both HCC types. KDM6B is an epigenetic regulator, which acts as a histone H3 lysine-27 (H3K27) demethylase that induces transcriptional gene activation^[15]. Downregulation of *Kdm6b* expression in the liver causes intrinsic defects in β -oxidation and, thereby, induces hepatosteatosis and glucose-insulin intolerance, suggesting that *Kdm6b* regulates energy homeostasis in the liver^[16]. Here, we demonstrate the molecular mechanism by which KDM6B loss epigenetically downregulates the expression of *G0S2*, a selective inhibitor of adipose triglyceride lipase/patatin like phospholipase domain containing 2 (ATGL/PNPLA2), in HCC cells, leading to increased resistance to lipotoxicity. We also show that the loss of KDM6B-*G0S2* is common in human NAFLD-related HCC.

METHODS

Human tissue samples

A total of 87 patients who underwent curative hepatic resection for HCC between 2006 and 2012 at Tokyo Medical and Dental University Hospital with approval of the ethics committees (permission number; G2017-018) of the Faculty of Medicine in Tokyo Medical and Dental University were collected, and written informed consent was obtained from all patients. The patients were anonymously coded in accordance with ethical guidelines, as instructed by the Declaration of Helsinki and Istanbul.

Cell lines and reagents

Human HCC cell lines (HuH7, JHH5, HLE, and HLF) were purchased from the American Type Culture Collection (Manassas, VA) and the Human Science Research Resources Bank (Osaka, Japan). Cells were cultured in an appropriate culture medium (Supporting Information, <http://links.lww.com/HC9/A541>) under 5% CO₂ at 37°C. These cell lines were authenticated by DNA fingerprinting of short tandem repeats (BEX Co. Ltd, Tokyo, Japan). Cells were tested with a mycoplasma contamination detection assay before the experiment. Palmitate (Merck KGaA, Darmstadt, Germany) stock solution was prepared

by coupling palmitate to bovine serum albumin (BSA; Merck KGaA, Darmstadt, Germany) as previously described^[17]. ATGL/PNPLA2 inhibitor, Atglistatin (Selleck Biotech, Houston, TX), was dissolved in DMSO and used at a concentration of 0, 10, or 50 μM ^[18].

5hmC detection

5hmC was analyzed using the EpiMark 5hmC and 5-mC analysis kit (E333175; New England Biolabs, New England Biolabs, Ipswich, MA) according to the manufacturer's instructions. Briefly, genomic DNA was incubated with the T4 β -glucosyltransferase that protects against Msp1 digestion (CCGG) by adding a glucose moiety specifically to 5hmC^[19]. The 5hmC was detected by glycosylated hydroxymethyl-sensitive PCR using primers designed around the analyzed Msp1 digestion sites. The primer sequences are shown in Supplemental Table S1 (<http://links.lww.com/HC9/A539>).

RNA interference

HuH7 and JHH5 cells were transfected with small interfering RNAs (siRNAs) for *KDM6B* (SASI_Hs02_00314716, SASI_Hs02_00314717; Merck KGaA), *G0S2* (SASI_Hs01_00133110, SASI_Hs02_00348390), *ACSL1* (SASI_Hs01_00202187, SASI_Hs01_00202188), *ATGL/PNPLA2* (SASI_Hs01_00225605, SASI_Hs01_00225606), or with negative control (MISSION siRNA Universal Negative Control; Merck KGaA) using Lipofectamine RNAiMAX Transfection Reagent (Thermo Fisher Scientific, Waltham, MA) at a final concentration of 50 nM.

Establishment of *KDM6B*-KO cell lines

The CRISPR-targeting sequences (5'-CACAGCGCCC TTCGATACGGAGG-3') were designed based on the Optimized CRISPR Design web system (<http://crispr.mit.edu/>). Oligos were cloned into the gRNA Cloning Vector (plasmid #41824; Addgene Addgene, Watertown, MA) following CRISPR gRNA Synthesis Protocol^[20] and transfected with the hCas9 (Addgene; plasmid #41815). After transfection of the vectors into HuH7 and JHH5 cells and selection by G418, Geneticin (Thermo Fisher Scientific), several *KDM6B*-KO clones were obtained by limiting dilution.

Quantitative reverse transcription PCR

Total RNA from the cultured cells was extracted using the RNeasy Protect Mini Kit (Qiagen). First-strand cDNA was synthesized from total RNA using the SuperScriptIII cDNA Synthesis kit (Thermo Fisher

Scientific). Quantitative reverse transcription PCR was performed using the TB Green Premix Ex Taq kit (Takara Bio, Shiga, Japan) and gene-specific primers in the StepOne real-time PCR System (Thermo Fisher Scientific). Sequences of primers are presented in Supplemental Table S1 (<http://links.lww.com/HC9/A539>). Relative expression of mRNA was calculated using the comparative C_t method after normalization to *glyceraldehyde 3-phosphate dehydrogenase* expression. All experiments were conducted in triplicate and repeated at least twice.

Microarray analysis

The integrity of the obtained RNA was confirmed by using a 2100 Bioanalyzer (Agilent Technologies, Santa Clara, CA). Complementary RNA was prepared from 100 ng of total RNA from each sample with a 3' IVT Express Kit (Affymetrix Santa Clara, CA). Hybridization and signal detection of the Gene Chip Human Genome U133 Plus 2.0 Array (Affymetrix) were performed in accordance with the manufacturer's instructions. The microarray datasets of pairs of the *KDM6B* wild-type (WT) and *KDM6B*-KO cells were normalized using the robust multiarray average method in the R statistical software and Affy Bioconductor package.

Western blotting

Cells were washed with PBS for total cell lysis and dissolved in an RIPA buffer (Thermo Fisher Scientific) with a protease inhibitor cocktail (Merck KGaA). After SDS-PAGE, the proteins were transferred onto polyvinylidene difluoride membranes (Immobilon-P; Merck KGaA). The membranes were probed overnight with first primary antibodies for *KDM6B* (Cell Signaling Technology), *G0S2* (Abcam, Cambridge, UK), *ACSL1* (Cell Signaling Technology), *ATGL/PNPLA2* (Cell Signaling Technology), α -tubulin (Santa Cruz Biotechnology, Dallas, TX), or glyceraldehyde 3-phosphate dehydrogenase (Cell Signaling Technology). Goat antirabbit or antimouse IgG (H/L) with horseradish peroxidase-labeled secondary antibodies were used for visualization using the Western ECL substrate kit (BioRad Laboratories, Hercules, CA). The antibodies used for western blotting are listed in Supplemental Table S2 (<http://links.lww.com/HC9/A539>).

Lipidome analysis

Lipidome analysis was performed according to the Lipidome Lab Nontargeted Lipidome Scan package (Lipidome Lab, Akita, Japan) using liquid chromatograph orbitrap mass spectrometry, as shown in Supporting

Information (<http://links.lww.com/HC9/A541>). The raw data files were postprocessed using the Lipid Search 4.2 software (Mitsui Knowledge Industries Co. Ltd, Tokyo, Japan), which identified individual intact lipid molecules. The relative values were calculated using the ratio of the chromatographic peak area of each analyte to that of the total analyte. The annotation method corresponds to an equivalent of the “Fatty Acyl/Alkyl Level or Hydroxyl Group Level” that is defined by the Lipidomics Standard Initiative^[21].

Lipid quantification

Intracellular lipids were extracted using the Lipid Extraction Kit (Cell Biolabs Inc., San Diego, CA) and then solubilized in a 100 μ L methanol/chloroform mixture. Triglycerides were quantified using the Lipid Quantification Kit (Fluorometric) (Cell Biolabs Inc.), according to the manufacturer’s protocol.

Lipid staining

For neutral lipid and cholesteryl ester staining, cells were fixed with 4% paraformaldehyde and stained with Oil red O (Merck KGaA) as described previously^[22]. Lipids were quantified using the ImageJ software (National Institutes of Health).

Cell proliferation assay

Cell viability was evaluated by a WST-8 assay using the Cell Counting Kit-8 (Dojindo, Kumamoto, Japan). Briefly, cells were plated at a density of 5.0×10^3 cells per well in 96-well plates and cultured for 48 hours. Cells were incubated in a fresh culture medium containing 10% Cell Counting Kit-8 reagent for 2 hours under 5% CO₂ at 37°C. Absorbance was evaluated at 450 nm using a spectrophotometer (iMark; BioRad Laboratories). To assess the lipotoxic effects, the cell reduction rate was determined as the ratio of viable cells of the palmitate-treated and palmitate-untreated (control) groups after 48 hours of incubation.

Chromatin immunoprecipitation (ChIP)

ChIP assay was performed by using the ChIP-IT Express Kit (Active Motif, Carlsbad, CA) according to the manufacturer’s protocol. The antibodies used in this study were anti-H3K27me3 (Active Motif) and anti-KDM6B (Cell Signaling Technology). Anti-PanH3 (Merck KGaA) and input DNA samples were used as internal controls. The primer sequences of ChIP-PCR are listed in Supplemental Table S1 (<http://links.lww.com/HC9/A539>).

ATGL activity measurement

ATGL activity was assessed using the EnzChek lipase substrate (Thermo Fisher Scientific). ATGL cell extracts from 7.0×10^6 cells were prepared in 300 μ L of enzyme reaction buffer (50 mM HEPES, pH 7.2, 100 mM NaCl, 5 mM CaCl₂, 0.5 mM DTT, 2% DMSO, and 0.1% Triton X-100). The ATGL activity assay was conducted in a 96-well plate containing 100 μ g of ATGL cell extracts. The EnzChek lipase substrate was added to each well to a final concentration of 1 μ M to initiate the reaction at 37°C. Fluorescence (excitation: 485 nm and emission: 510 nm) was recorded every 30 seconds for 90 minutes using Varioskan LUX (Thermo Fisher Scientific).

Bioinformatics analysis

The human and mouse microarray datasets, previously deposited in Gene Expression Omnibus (GSE102083), were used for this study. For analyzing human microarray data, 32 pairs of HCC and adjacent liver tissues surgically resected from NBNC patients were extracted. The microarray data were normalized using the robust multiarray average method in R statistical software and the Affy Bioconductor package. Public transcriptome data of HCC tissues and adjacent liver tissues were obtained from The Cancer Genome Atlas (TCGA) Research Network and downloaded from the cBioPortal site. Gene set enrichment analysis was performed using MSigDB gene sets^[23].

Immunohistochemistry

As described previously, formalin-fixed and paraffin-embedded tissues of human and *MC4R*^{-/-} mouse HCC samples were used for immunohistochemistry^[9]. The tissue sections were incubated with primary antibodies against KDM6B (Abcam) and G0S2 (Abcam) overnight at 4°C (Supplemental Table S2, <http://links.lww.com/HC9/A539>). After reaction with the Histofine Simple Stain MAX PO system (Nichirei Biosciences, Tokyo, Japan) for 1 hour at 20°C, immunoreactivity was visualized with 3-3'-diaminobenzidine (Wako, Osaka, Japan), followed by counterstaining with Mayer hematoxylin (Wako). The KDM6B expression in HCC tissues was determined as high and low according to the percentage of positive cells and intensity of the nuclear staining^[14,24]. The percentage of positive cells was scored as follows; 0, no positive cells; 1, 1%–25%; 2, 26%–50%; 3, 51%–75%; and 4, 76%–100%. Positive staining intensity was graded according to the mean density; 0, negative; 1, weak; 2, moderate; and 3, strong. KDM6B expression was divided into low (score 0–4) and high (score 5–12) based on the staining score calculated as the multiplication of 2 scores. According to a previous report, cytoplasmic G0S2

expression in HCC was also defined as high and low^[25]. Since KDM6B and G0S2 were expressed in normal liver tissues, we also determined low expression when their expression levels in HCC tissues were lower than those in adjacent nontumor liver tissues.

Statistical analysis

Statistical analysis was performed using R statistical software and Microsoft Excel for Mac 2019. Welch *t* test was used to analyze the differences between the continuous values of the 2 independent groups. The χ^2 test was used for the analysis of categorical variables. For all analyses, *p* values <0.05 were considered statistically significant.

RESULTS

KDM6B expression is downregulated in NBNC and MC4R^{-/-} mouse HCCs

Using our previous dataset, we reanalyzed the expression levels of epigenetic regulator genes between human and MC4R^{-/-} mouse HCC (Figure 1A, upper panels, <https://www.ncbi.nlm.nih.gov/geo>; accession number GSE102083). Microarray analysis detected 12 downregulated epigenetic regulator genes in human NBNC-HCC samples and 16 downregulated epigenetic regulator genes in MC4R^{-/-} mouse HCC (Figure 1A, B). In contrast, 66 upregulated epigenetic regulator genes were found in human NBNC-HCC, and 16 upregulated epigenetic genes were found in MC4R^{-/-} mouse HCC (Figure 1A, B). KDM6B was downregulated in human HCC tissues among the common genes detected using the microarray in this study (Figure 1A, lower panels). We used public data to confirm the findings of our microarray data. Public transcriptome data provided by TCGA Research Network showed a lower expression level of KDM6B in nonviral HCC than in adjacent liver tissues (Figure 1C, left panel, $p = 7.00 \times 10^{-15}$), which was consistent with our human nonviral (Figure 1C, middle panel, $p = 4.46 \times 10^{-5}$) and mouse MC4R^{-/-}-HCC data (Figure 1C, right panel, $p = 0.018$). Immunohistochemical analysis confirmed the loss of KDM6B protein expression in human NAFLD-related HCC of the nonviral type and mouse HCC tissues (Figure 1D), both of which had low KDM6B expression in our microarray analysis.

KDM6B expression correlates with 5hmC levels at the gene body region

In human HCC cell lines, KDM6B mRNA expression was high in HuH7 and JHH5 cells but low in HLE and HLF cells (Figure 2A). It has recently been reported that

a gain of 5hmC at the CpG island located within exons 17 to 18 correlates with increased *Kdm6b* expression in mouse neural cells^[26] (Figure 2B). Since human genomic KDM6B contains a region with high sequence homology to the mouse putative *Kdm6b* regulatory region, we evaluated the 5hmC levels at the conserved region by glycosylated hydroxymethyl-sensitive PCR. HuH7 and JHH5 cells with high KDM6B expression exhibited detectable levels of 5hmC at 2 CpG sites, while HLE and HLF cells with low KDM6B expression did not, suggesting that the regulation of KDM6B expression may depend on the 5hmC levels at the region (Figure 2C).

KDM6B-KO reduces gene expression in lipid metabolism pathways and increases resistance to lipotoxicity in HCC cells

To clarify the role of KDM6B dysfunction, we established the KDM6B-KO subclone from HuH7 and JHH5 cells using the CRISPR-cas9 system (Figure 2D, Supplemental Figure S1, <http://links.lww.com/HC9/A540>), and then, genome-wide expression analysis between KDM6B-WT HuH7 cells and KDM6B-KO HuH7 cells by DNA microarrays was conducted. Gene set enrichment analysis demonstrated that Myc-targets, mTORC1-signaling, and metabolic pathways were suppressed when KDM6B was knocked out (Supplemental Table S3, <http://links.lww.com/HC9/A539>). Among them, the inhibition of gene signatures involved in the cholesterol and fatty acid metabolism pathways was noted in KDM6B-KO HuH7 cells (Figure 2E, Supplemental Table S3, <http://links.lww.com/HC9/A539>, normalized *p* values of 0.002 and 0.025, respectively). As hepatic lipid accumulation is an important feature of NAFLD^[1] and MC4R^{-/-} mice^[8], we further studied the effects on cellular metabolites, especially lipid metabolism, due to the addition of fatty acids in KDM6B-KO cells by lipidome analysis. Principal component analysis of the 1059 molecular species revealed a clear difference in lipid profiles between KDM6B-WT and KDM6B-KO cells under vehicle and palmitate treatment (Figure 2F). Notably, metabolites that specifically reduced in KDM6B-KO cells (\log_2 fold change < -0.5 and $p < 0.05$) were predominantly composed of triglyceride species (vehicle, $p = 1.15 \times 10^{-4}$; palmitate, $p = 2.07 \times 10^{-40}$, Figure 2G). In addition, a subset of 106 molecular species (including 55 molecular species corresponding to triglyceride) exhibited marked accumulation in KDM6B-WT cells compared to KDM6B-KO cells upon palmitate treatment (Figure 2H, Supplemental Table S4, <http://links.lww.com/HC9/A539>), with 6 representative molecular species of triglyceride exemplified in Figure 2I. We subsequently performed lipid quantification using the 2 cell lines and validated that the intracellular triglyceride level in KDM6B-KO cells was lower than that in KDM6B-WT cells under palmitate treatment ($p < 0.05$, Figure 2J).

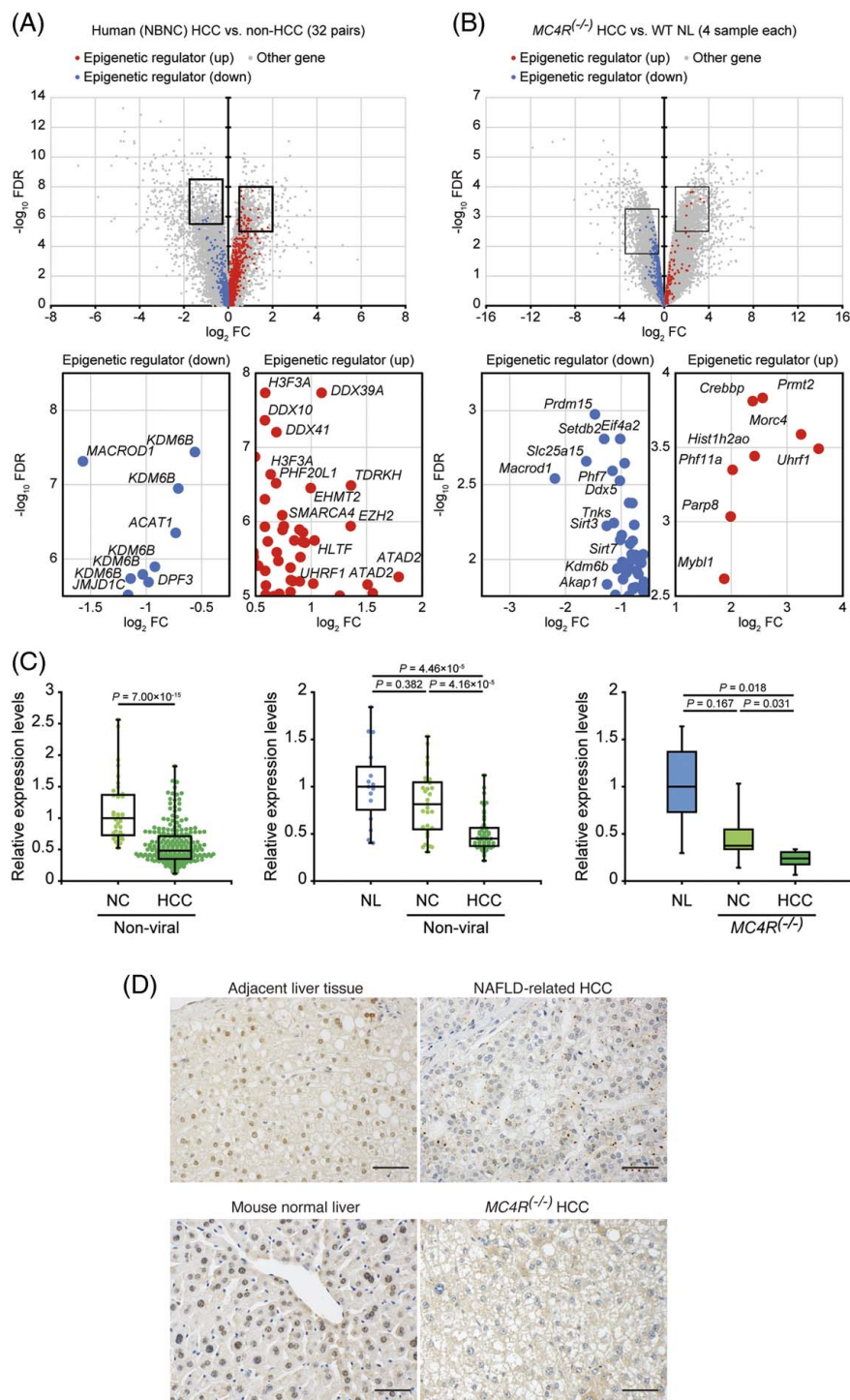
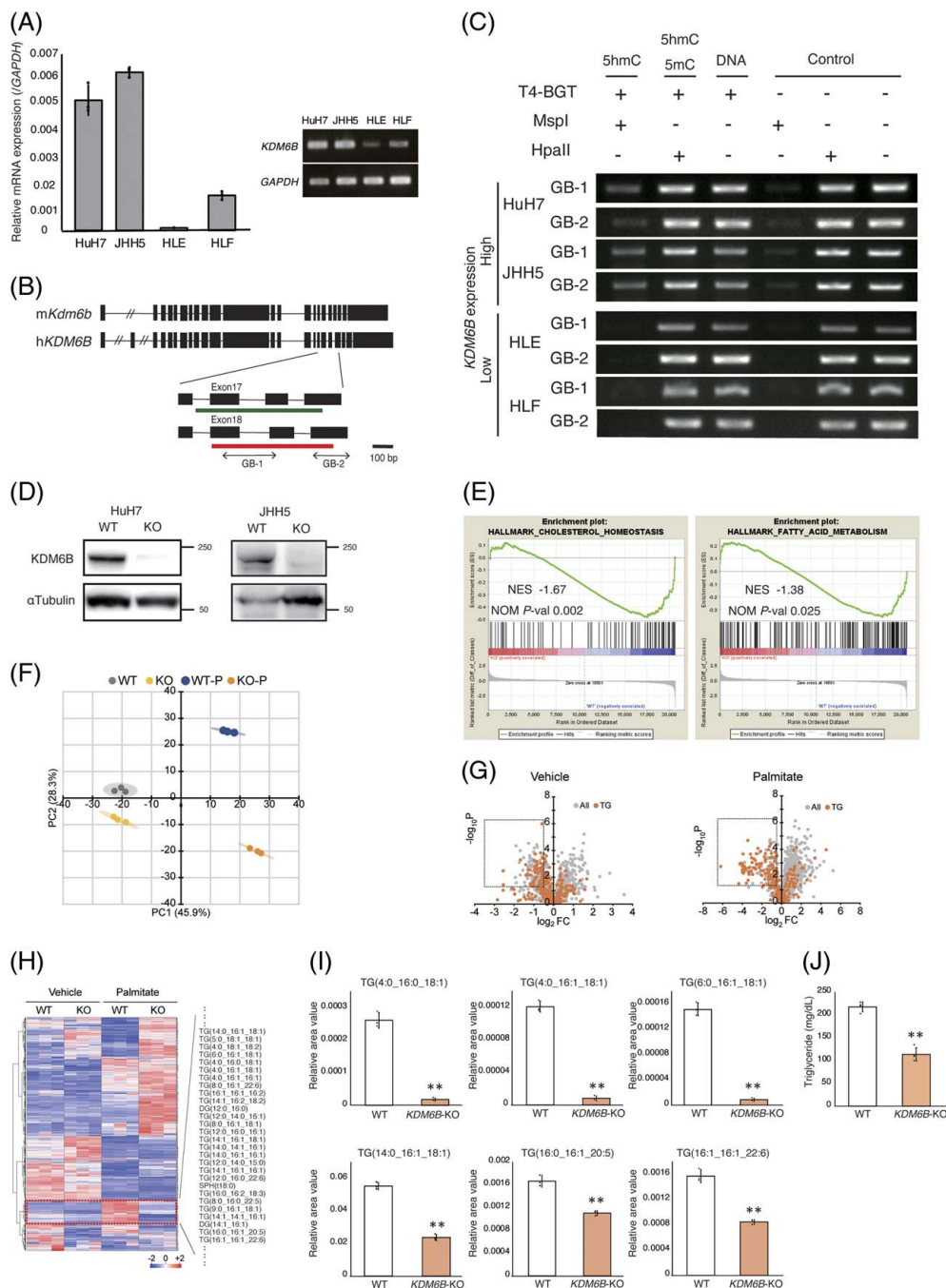


FIGURE 1 Identification of differentially expressed genes and *KDM6B* expression levels in human and mice. (A) Volcano plot of differentially expressed gene between NBNC-HCC and non-HCC in humans. (B) Volcano plot of differentially expressed gene between *MC4R*^{-/-} HCC and *MC4R*^{+/+} (wild-type) normal livers in mice. Representative upregulated and downregulated genes are shown in the lower panel. Blue dots indicated 21 downregulated ($|\log_2FC| > 1.5$ and $FDR < 0.001$) probes in humans and 19 downregulated ($|\log_2FC| > 1$ and $FDR < 0.05$) probes in mice, respectively. Red dots indicated 93 upregulated ($|\log_2FC| < 1.5$ and $FDR > 0.001$) probes in humans and 16 upregulated ($|\log_2FC| < 2$ and $FDR > 0.05$) probes in mice, respectively. (C) Box and beeswarm plots of *KDM6B* expression levels in humans and mice. The left, middle, and right panels show TCGA, human data, and mice data, respectively. Boxes represent the interquartile range (range from the 25th to 75th percentile), and horizontal lines show the median values. p values were calculated using the Mann-Whitney U test. (D) Immunohistochemical staining of *KDM6B* in human NAFLD-related HCC and *MC4R*^{-/-} HCC tissues used in microarray analysis (Figure 2C, middle and right). NAFLD-HCC and *MC4R*^{-/-} HCC exhibited low *KDM6B* expression compared to human liver tissue adjacent to NAFLD-HCC and normal mouse liver tissue, respectively. Magnification: $\times 200$; scale bar: 50 μ m. Abbreviations: FC, fold change; FDR, false discovery rate; *MC4R*, melanocortin type 4 receptor; NBNC-HCC, HBV surface antigen-negative and HCV antibody-negative HCC; NC, adjacent liver tissues; NL, normal liver tissues; TCGA, The Cancer Genome Atlas.



Next, we investigated the biological changes in cells by adding palmitate. Oil red O staining showed lipid accumulation when *KDM6B*-WT HCC cells were treated with a 300 μ M (HuH7) or 150 μ M (JHH5) dose of palmitate^[27,28]. Lipid accumulation in the *KDM6B*-KO cells was lower than that in *KDM6B*-WT cells (Figure 3A, $p < 0.05$). We then performed a cell proliferation assay to evaluate the lipotoxicity in *KDM6B*-KO cells treated with palmitate. Reduction rates of *KDM6B*-KO cells upon the addition of palmitate were significantly lower than those of WT cells (Figure 3B, $p < 0.01$), indicating that *KDM6B*-KO cells may increase resistance to lipotoxicity^[29]. Similarly, decreased lipid accumulation and reduction rates were

observed in HuH7 cells when *KDM6B* expression was inhibited by siRNA treatment (Supplemental Figure S2A–C, <http://links.lww.com/HC9/A540>).

Increased H3K27 trimethylation at the promoter regions of *G0S2* and *ACSL1* in *KDM6B*-KO cells

Microarray analysis detected 30 downregulated ($< 2^{-2}$ fold) probes in the *KDM6B*-KO HuH7 cells when compared to that of *KDM6B*-WT cells (Supplemental Table S5, <http://links.lww.com/HC9/A539>, <https://www>.

FIGURE 2 *KDM6B* knockout effects in HuH7 and JHH5 cells. (A) Endogenous relative expression of *KDM6B* in human liver cell lines. The relative mRNA expression levels were calculated using the comparative C_t method and normalization to *GAPDH*. Data from repeated triplicate experiments were averaged and expressed as mean \pm SD. Each measurement is shown in a scatter plot. (B) Structure of the mouse and human *KDM6B* gene. Black squares indicate exons. The green bar indicates the mouse CG-rich region that is reported to show a positive correlation between *KDM6B* expression and 5hmC^[25]. Red bars indicate CpG islands registered in the UCSC genome browser (<https://genome.ucsc.edu/>). PCR was performed at the gene body region indicated by bilateral arrows (GB-1 and GB-2). (C) Comparison of 5hmC levels in the CpG island in the gene body of *KDM6B* in HCC cell lines. *KDM6B* expression epigenetically correlates with 5hmC levels in the gene body. (D) Western blot analysis of *KDM6B* and α -tubulin in WT control cells and *KDM6B*-KO clones. (E) Gene expression analysis of *KDM6B*-KO HuH7 cells. Enrichment plots of gene sets associated with lipid metabolism. (F) Plot of principal component analysis of lipidome assay data using liquid chromatograph orbitrap mass spectrometry. Ellipses indicate groups of *KDM6B*-WT and KO cells with/without palmitate treatment and represent +3 SD. (G) Volcano plots of differentially detected metabolites between the *KDM6B*-WT and *KDM6B*-KO cells. Boxed areas contain the metabolites with significantly decreased levels in the *KDM6B*-KO cells ($\log_2FC < -0.5$, $p < 0.05$). Left panel: vehicle; right panel: treated with palmitate. (H) Heatmap of metabolites detected using lipidome assay. FC were calculated from the mean values of HuH7 *KDM6B*-WT and *KDM6B*-KO cells. p values were calculated using Welch t test. Z scores were calculated for each lipid, and principal component and clustering analyses were performed using Python with Matplotlib and Seaborn packages. (I) Candidate metabolites. Data are expressed as mean \pm SD. Each measurement is shown in a scatter plot ($n = 3$). (J) Quantification of intracellular triglyceride levels. Data are expressed as mean \pm SD. Each measurement is shown in a scatter plot ($n = 3$). ** $p < 0.01$. Abbreviations: FC, fold change; *GAPDH*, glyceraldehyde 3-phosphate dehydrogenase; GB, gene body; 5hmC, 5-hydroxymethylcytosine; h*KDM6B*, human *KDM6B*; KO, knockout; KO-P, *KDM6B*-knockout cells with palmitate treatment; m*Kdm6B*, mouse *Kdm6b*; NES, normalized enrichment score; NOM P -val, nominal p value; PC, principal component; TG, triglyceride; WT, wild-type; WT-P, *KDM6B* wild-type cells with palmitate treatment.

ncbi.nlm.nih.gov/geo/; accession number GSE211848). Among them, 6 known lipid metabolism-related genes (*SLC22A3*, *CCDC22*, *ABAT*, *AHSG*, *ACSL1*, and *G0S2*) were selected, and then, mRNA expression levels were validated by quantitative reverse transcription PCR analysis. The HuH7 and JHH5 cells with *KDM6B*-KO showed significantly decreased expression levels of 6 genes, except *CCDC22* in JHH5 cells (Figure 3C, $p < 0.01$). Moreover, mRNA levels of the 3 target genes (*ABAT*, *ACSL1*, and *G0S2*) were commonly downregulated by *KDM6B* knockdown in HuH7 and JHH5 cells (Supplemental Figure S2D, <http://links.lww.com/HC9/A540>, $p < 0.05$).

To clarify how *KDM6B* regulates downstream target gene expression, we quantified *KDM6B* occupancy and H3K27me3 levels at the promoter region of 3 genes (*ABAT*, *ACSL1*, and *G0S2*) between *KDM6B*-WT and KO cells. A ChIP assay using anti-*KDM6B* antibodies demonstrated that *KDM6B* was significantly recruited at the promoter region of *ACSL1* and *G0S2* in *KDM6B*-WT cells (Figure 3D, E, $p < 0.01$). The H3K27me3 levels at the promoter regions of *ACSL1* and *G0S2* were higher in *KDM6B*-KO cells than those in *KDM6B*-WT cells (Figure 3F, $p < 0.05$). However, *KDM6B* occupancy and H3K27me3 levels were changed at the *ABAT* promoter region in JHH5 cells but not in HuH7 cells after *KDM6B*-KO. These data indicate that *KDM6B* can bind the promoter regions of the lipid metabolism-related genes, *ACSL1* and *G0S2*, and induce H3K27 demethylation, resulting in positive regulation of these gene expressions.

***KDM6B*-KO reduces lipid accumulation and gains lipotoxicity resistance by suppressing *G0S2* expression**

To investigate whether *KDM6B*-KO-mediated reduction of lipid accumulation is due to the decreased expression of *G0S2* and *ACSL1*, we silenced the expression of

G0S2 and *ACSL1* by siRNA in HuH7 and JHH5 cells (Figure 4A, B, Supplemental Figure S3A, B, <http://links.lww.com/HC9/A540>). Lipid accumulation in HuH7 and JHH5 cells was significantly lower in cells transfected with *G0S2* or *ACSL1* siRNA than in cells transfected with negative control siRNA, followed by palmitate treatment (Figure 4C, Supplemental Figure S3C, <http://links.lww.com/HC9/A540>, $p < 0.01$). Suppression of *G0S2* expression showed resistance to lipotoxicity (Figure 4D, $p < 0.05$), whereas suppression of *ACSL1* expression did not (Supplemental Figure S3D, <http://links.lww.com/HC9/A540>). Rescued *G0S2* expression in *KDM6B*-KO cells increased lipid accumulation and the cell reduction rate (Supporting Information, Supplemental Figure S4, <http://links.lww.com/HC9/A540>), suggesting that reduced lipid accumulation and enhanced resistance to lipotoxicity by *KDM6B*-KO may be due to the decreased expression of *G0S2*.

Decreased lipid accumulation and acquired resistance to lipotoxicity by loss of *KDM6B*-*G0S2* are mediated by ATGL/PNPLA2

G0S2 specifically interacts with the intracellular triglyceride hydrolyzing enzyme ATGL/PNPLA2 and inhibits the lipolytic enzyme activity of ATGL^[30]. ATGL/PNPLA2 hydrolyzes intracellular triglycerides, stored in lipid droplets, to fatty acids^[31]. To determine whether the reduction of lipid accumulation and acquisition of lipotoxicity by *KDM6B*-KO are due to enhanced ATGL/PNPLA2-dependent lipolysis caused by *G0S2* downregulation, we examined the role of ATGL/PNPLA2 in HCC cells. A fluorescence-based ATGL activity assay demonstrated that ATGL activity in *KDM6B*-KO cells was higher than that in WT cells (Figure 5A). Similarly, *G0S2*-knockdown *KDM6B*-WT cells also increased ATGL activity compared with the negative control-transfected cells (Figure 5B).

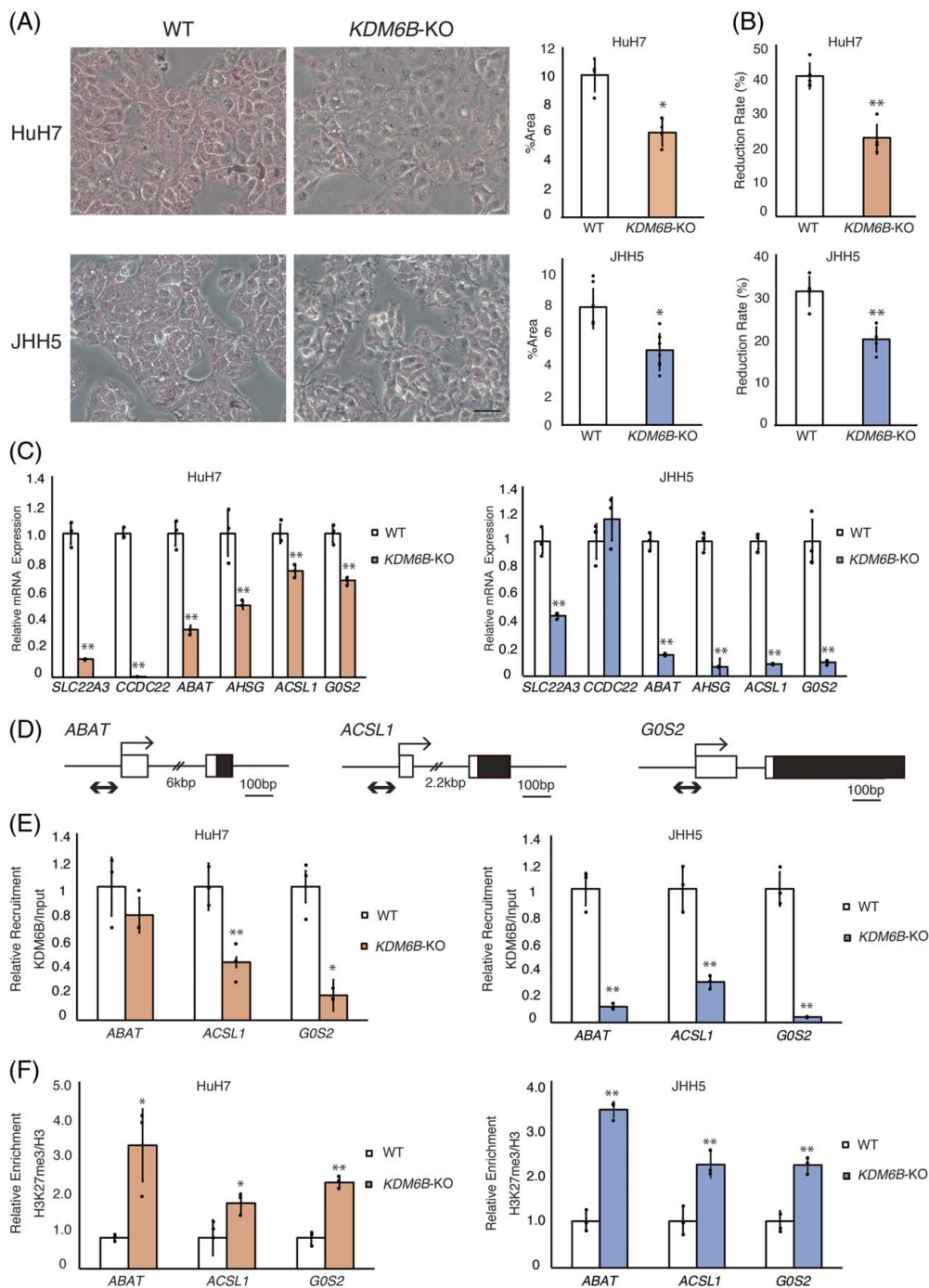


FIGURE 3 Knockout of *KDM6B* reduces lipid accumulation and increases lipotoxicity resistance. (A) Lipid accumulation in HuH7 and JHH5 followed by 48 hours of palmitate treatment (HuH7: 300 μ M and JHH5: 150 μ M). Visualization and quantification of lipids by Oil Red O staining. Scale bar: 100 μ m. Five different fields were imaged by a microscope. The percentage of Oil-red-O-stained area in cells was calculated using the ImageJ software. (B) Cell proliferation evaluated by WST assay. The reduction rates of WT and KO cells were calculated by cell proliferation rate with and without palmitate treatment after 48 hours of incubation ($n = 4$). (C) Identification of target genes of *KDM6B* by epigenetic regulation. Quantitative reverse transcription PCR analysis of metabolism-related genes downregulated by *KDM6B*-KO in the HuH7 and JHH5 cells ($n = 3$). (D) The promoter regions of the 3 genes are shown. Transcriptional start sites are indicated by arrows, exons by squares, 5' untranslated regions by white squares, and translated regions by black squares. ChIP-PCR was performed at the promoter regions indicated by bilateral arrows. (E) Quantitative ChIP analysis of candidate metabolism-related genes downregulated by *KDM6B*-KO in HuH7 and JHH5 cells. HuH7: left panel; JHH5: right panel. The enrichment levels of KDM6B at the promoter region were commonly decreased in *AHSG*, *ACSL1*, and *GOS2* ($n = 3$). (F) Quantitative ChIP analysis of candidate genes regulated by KDM6B. HuH7: left panel; JHH5: right panel. The enrichment levels of H3K27me3 at the promoter region were commonly increased in *ACSL1* and *GOS2* ($n = 3$). Data from repeated experiments were performed in triplicate. All values are represented as the mean \pm SD. Each measurement is shown in a scatter plot. * $p < 0.05$; ** $p < 0.01$. Abbreviations: ChIP, chromatin immunoprecipitation; KO, knockout; WT, wild-type.

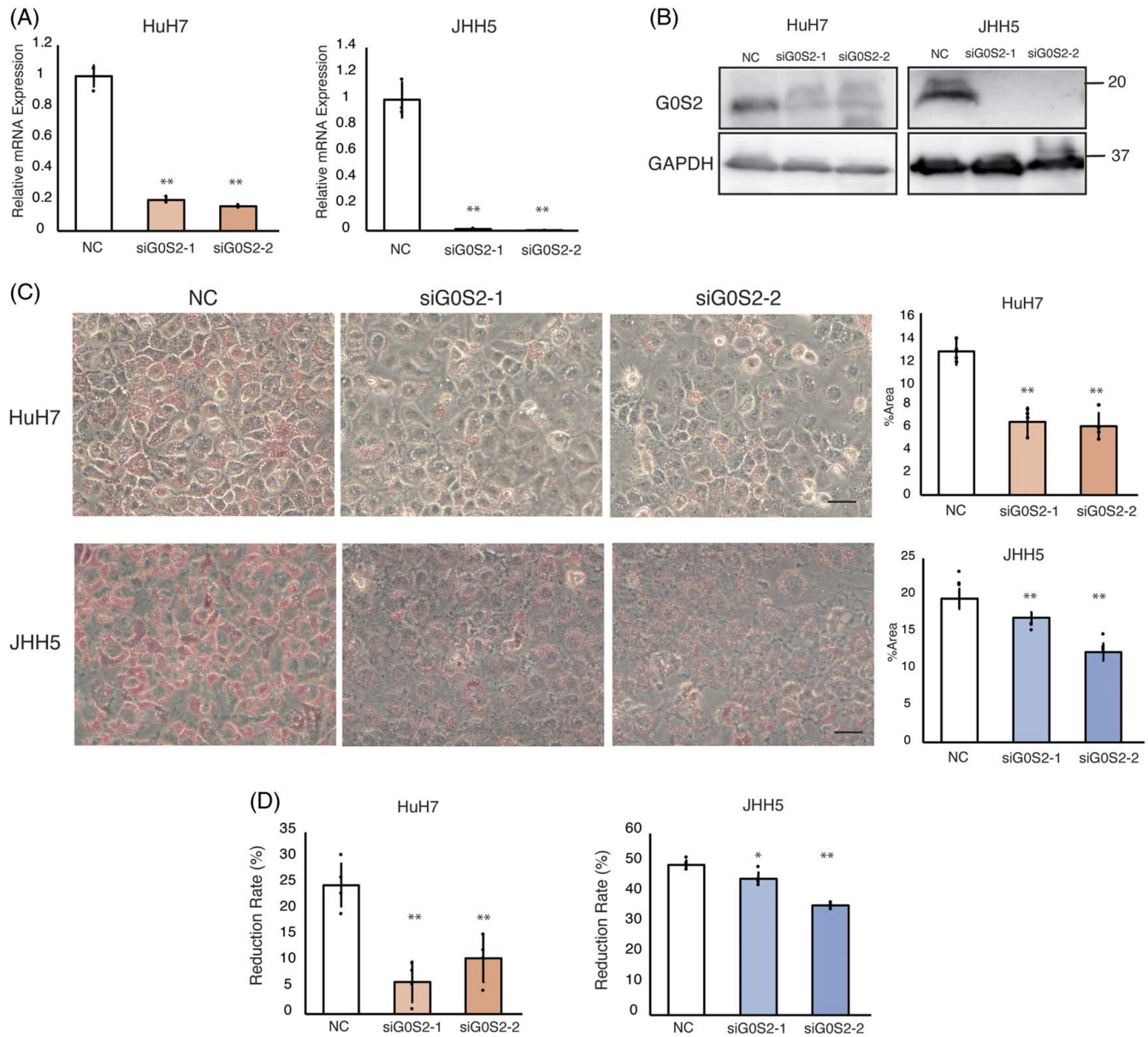


FIGURE 4 Knockdown of *G0S2* reduces lipid accumulation and increases resistance to lipotoxicity. HuH7 and JHH5 cells were treated with control or *G0S2* small interfering RNA at 50 nM concentration for 48 hours. (A) Changes in *G0S2* mRNA levels ($n = 3$). (B) Western blot analysis for *G0S2* and GAPDH in HuH7 and JHH5 cells. (C) Under the conditions described in (A) and (B), cells were stained with Oil Red O and evaluated for proliferation, followed by palmitate treatment for 48 hours (HuH7: 300 μ M and JHH5: 150 μ M). Scale bar: 100 μ m. The percentage of Oil-red-O-stained area in cells was calculated from 3 representative locations using the ImageJ software. (D) Cell proliferation evaluated by WST assay. The reduction rate was calculated as described in Figure 3 ($n = 5$). All values are represented as the mean \pm SD. Each measurement is shown in a scatter plot. * $p < 0.05$; ** $p < 0.01$. Abbreviations: GAPDH, glyceraldehyde 3-phosphate dehydrogenase; NC, negative control.

We then performed *ATGL/PNPLA2* knockdown in HuH7 *KDM6B*-KO cells (Figure 5C, D), and the suppression of *ATGL/PNPLA2* expression increased lipid accumulation in *KDM6B*-KO cells (Figure 5E, $p < 0.01$). Similarly, treatment with Atglistatin, a selective inhibitor of *ATGL/PNPLA2*, showed significantly higher lipid accumulation in *KDM6B*-KO cells compared to that in control cells (Figure 5F, $p < 0.05$). In contrast, *ATGL/PNPLA2* knockdown or Atglistatin treatment showed significant inhibition of cell proliferation of

KDM6B-KO cells compared to that in control cells (Figure 5G, $p < 0.01$). However, there was no apparent effect of the suppression of *ATGL/PNPLA2* or Atglistatin on lipid accumulation or cell proliferation in *KDM6B*-WT cells (Supplemental Figure S5, <http://links.lww.com/HC9/A540>). These data suggest that the loss of *KDM6B* and resultant *G0S2* downregulation decrease lipid accumulation and acquire resistance to lipotoxicity through the activation of *ATGL/PNPLA2*.

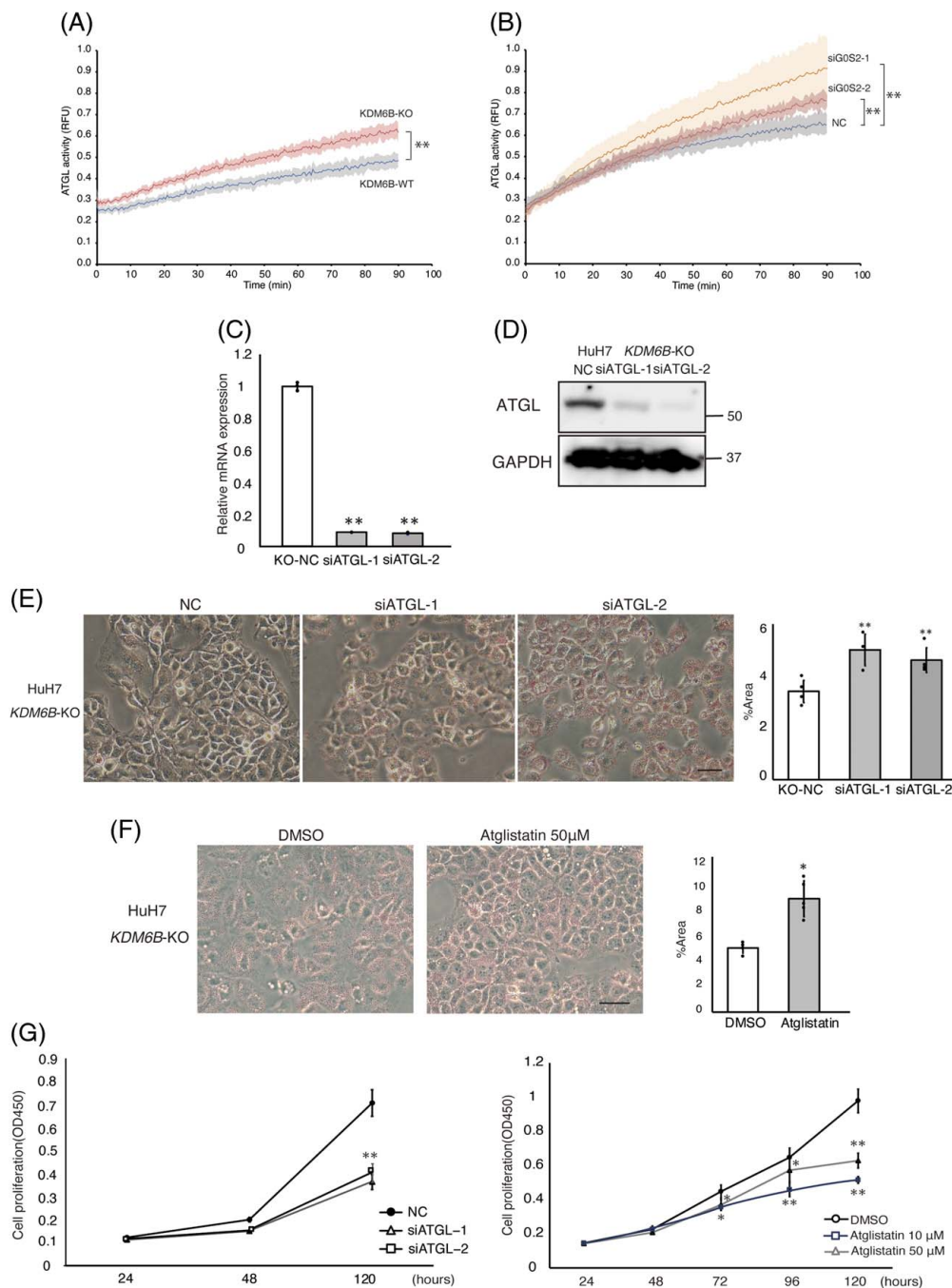


FIGURE 5 In HuH7 *KDM6B*-KO cells, suppression of ATGL/PNPLA2 expression, or pharmacological ATGL/PNPLA2 inhibition increases lipid accumulation and inhibits cell proliferation. (A) ATGL activity in HuH7 *KDM6B*-WT and KO cells. A fluorescence assay was performed to assess ATGL enzyme activity, which was recorded every 30 seconds for 90 minutes. Enzyme activity was measured twice or more for 1 sample and measured in 3 independent experiments. Solid lines indicate mean values; shaded areas indicate the 5%–95% interquartile range. Blue: HuH7 *KDM6B* WT and red: HuH7 *KDM6B* KO. ** $p < 0.01$. (B) ATGL activity in HuH7 *KDM6B*-WT cells with G0S2 knockdown. Gray: negative control small interfering RNA (NC); orange: siG0S2-1; and brown: siG0S2-2. ** $p < 0.01$. (C) Changes in *ATGL/PNPLA2* mRNA levels. Each measurement is shown in a scatter plot ($n = 3$). (D) Western blot analysis of ATGL/PNPLA2 and GAPDH. (E) *ATGL/PNPLA2* knockdown increases lipid accumulation analyzed by Oil Red O staining. (F) Representative images of HuH7 *KDM6B*-KO cells supplemented with Atglistatin, ATGL/PNPLA2 inhibitor, or DMSO, cultured for 5 days, fixed, and stained with Oil Red O are shown. Magnification: $\times 100$; scale bar: 100 μm . The percentage of Oil-red-O-stained area in cells was calculated in representative locations using the ImageJ software. Each measurement is shown in a scatter plot ($n = 5$). * $p < 0.05$; ** $p < 0.01$. (G) Left panel: growth curve is plotted for HuH7 *KDM6B*-KO cells treated with or without small interfering RNA against ATGL/PNPLA2. Right panel: growth curve for HuH7 *KDM6B*-KO cells in the presence or absence of Atglistatin. Cell proliferation was inhibited in a concentration-dependent manner by Atglistatin ($n = 5$). All values are represented as the mean \pm SD. * $p < 0.05$; ** $p < 0.01$. Abbreviations: ATGL, adipose triglyceride lipase; GAPDH, glyceraldehyde 3-phosphate dehydrogenase; KO, knockout; NC, Negative control; PNPLA2, patatin like phospholipase domain containing 2; WT, wild-type.

Low G0S2 expression in human HCC tissues is correlated with downregulated KDM6B expression

Finally, we evaluated the relationship between KDM6B and G0S2 expression in 87 human HCC specimens by immunohistochemistry. KDM6B expression was low in 25 of 87 HCC specimens (28.7%, Figure 6A, Table 1). The clinicopathological characters of the low KDM6B expression groups revealed the NBNC-HCC type (N = 20, 80%, $p < 0.001$). These findings were consistent with the data on our microarray and TCGA transcriptome analyses, which showed that *KDM6B* expression was downregulated in nonviral HCC (Figure 1C). Furthermore, the low KDM6B expression group was accompanied by NAFLD (N = 20, 80%, $p < 0.001$) and NASH (categorized as Matteoni type 3 and 4, N = 19, 76%, $p < 0.001$) that were pathologically diagnosed in the adjacent liver tissue. Moreover, adverse metabolic risk factors, such as obesity (N = 18, 72%, $p < 0.001$) and hypertension (N = 20, 80%, $p = 0.003$), were observed in the low KDM6B expression group.

G0S2 expression was reduced in 26 of 85 HCC tissues (30.5%, Figure 6B), which is associated with a high tumor number ($p = 0.022$, Supplemental Table S6, <http://links.lww.com/HC9/A539>). Decreased G0S2 expression cases significantly exhibited low KDM6B expression (N = 11, $p = 0.036$, χ^2 test, Supplemental Table S6, <http://links.lww.com/HC9/A539>). Moreover, the KDM6B/G0S2-double low expression group (N = 11) significantly correlated with NBNC ($p = 0.020$), NAFLD ($p < 0.001$), NASH ($p < 0.001$), obesity ($p = 0.001$), tumor size ($p = 0.016$), and tumor number ($p = 0.009$) in contrast to the KDM6B/G0S2-double high expression group (N = 47, Table 2).

DISCUSSION

In this study, we observed that KDM6B expression frequently decreased in NAFLD-related HCC. We used microarray and public database analyses to demonstrate that *KDM6B* transcription was downregulated in nonviral type HCC. Moreover, in patients with nonviral type HCC, KDM6B expression was significantly lower than that in adjacent liver tissues, which is consistent with the results of the TCGA database. Several factors such as STAT3, HOXC9, and miRNA^[32,33] are known to activate *KDM6B* expression at the transcriptional level. We found that *KDM6B* expression corresponded to 5hmC levels at the *KDM6B* gene body region in HCC cells, suggesting that this region is important for the regulation of *KDM6B* expression^[26]. A genome-wide analysis of liver 5hmC patterns in a mouse model of diet-induced obesity found that hepatic steatosis is associated with reversible 5hmC changes in numerous metabolic-related genes^[12]. Moreover, global DNA

hydroxy methylation levels in HCC are lower than those in non-neoplastic liver tissues^[34]. Aberrant DNA demethylation may be one of the mechanisms underlying KDM6B downregulation in our HCC cases.

In this study, according to gene set enrichment analysis, the metabolic pathways of cholesterol and fatty acids were suppressed in *KDM6B*-KO cells. Furthermore, a subset of the lipid metabolism-related metabolites including triglyceride molecular species was remarkably different in *KDM6B*-WT and *KDM6B*-KO cells treated with palmitate by lipidome analysis, and intracellular triglyceride levels were lower in *KDM6B*-KO cells than in WT cells. *Kdm6b* expression is decreased in the livers of mice exposed to a high-fat diet^[35]. Our results indicate that KDM6B is deeply involved in lipid metabolism, and the loss of KDM6B contributes to the development of NAFLD-related HCC. In addition, KDM6B transcriptionally activates global autophagy-network genes, such as *Tfeb* and *Atg7*, by decreasing H3K27me3 levels, thereby inducing autophagy-mediated lipid degradation in the livers of fasting mice^[36]. Moreover, fasting-induced KDM6B epigenetically upregulates the expression of β -oxidation-promoting genes, including *Fgf21*, *Cpt1a*, and *Mcad*^[16]. Here, we identified 2 novel KDM6B downstream target genes, G0S2 and *ACSL1*, which are directly regulated by KDM6B-dependent H3K27me3 demethylation at their promoter regions. G0S2, identified initially as a G0/G1 switch protein 2 in lymphocytes, plays a role in terminal differentiation and cell cycle progression^[37]. Recent studies indicate that the G0S2 protein content in the liver is increased in rats fed high-fat diets, promoting lipid accumulation by coupling with ATGL/PNPLA2 in the liver^[38,39]; this suggests that G0S2 is a lipid metabolism regulator. *ACSL1* facilitates the process of synthesizing triglycerides from fatty acids in hepatocytes^[40,41], especially in directing fatty acids toward mitochondrial β -oxidation^[42]. Both G0S2 and *ACSL1* knockdown inhibited lipid accumulation, but only the G0S2 knockdown demonstrated resistance to lipotoxicity. Our findings suggest that G0S2 downregulation in *KDM6B*-KO cells may explain the acquisition of lipotoxicity resistance.

G0S2 is a specific inhibitor of ATGL (also known as PNPLA2). ATGL/PNPLA2, a paralog of PNPLA3, is activated by binding to ABHD5, causing intracellular triglyceride hydrolysis^[43,44]. PNPLA3 also binds to ABHD5 but functionally competes with ATGL/PNPLA2 to prevent its activation and promote intracellular triglyceride deposition^[44]. A genome-wide association study analysis identified a genetic polymorphism of *PNPLA3* as a major risk for fatty liver disease^[45]. The PNPLA3 (I148M) variant has been shown to have a stronger functional competitive effect with ATGL/PNPLA2 than wild-type PNPLA3, resulting in the development of hepatic steatosis^[46,47]. In our study, *KDM6B*-KO cells possessed a high ATGL/PNPLA2

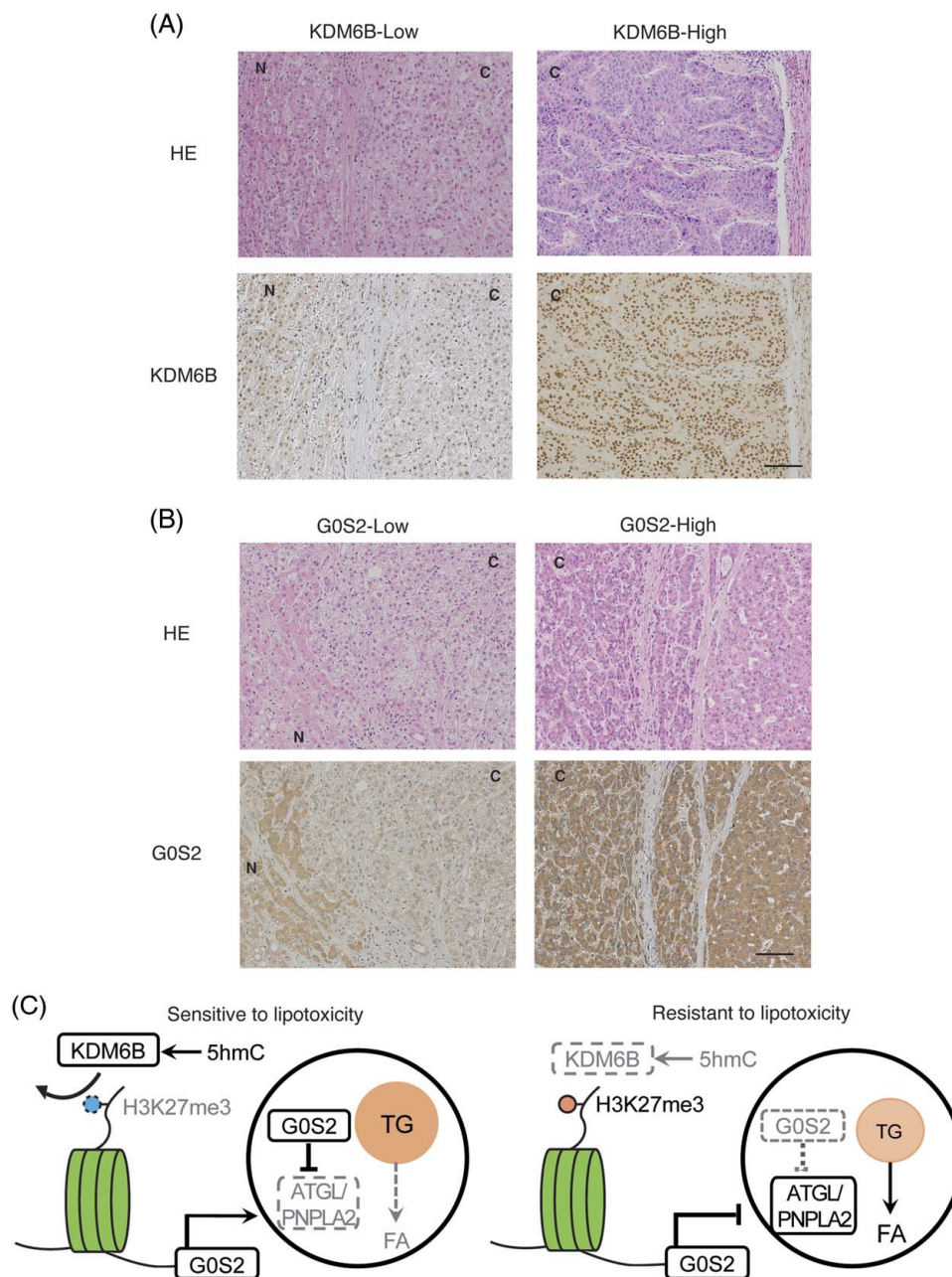


FIGURE 6 Immunohistochemistry evaluation of KDM6B and G0S2 expression. (A) HE staining and immunohistochemical analysis of KDM6B expression in HCC in representative KDM6B-high and KDM6B-low tissues. (B) Immunohistochemical staining of G0S2 in human HCC tissues. Low G0S2 expression was correlated with low KDM6B expression ($p = 0.036$). Magnification: $\times 100$; scale bar: 100 μm . (C) Schematic illustration of the regulation mechanism of intracellular lipid by KDM6B-G0S2-ATGL/PNPLA2 pathway. Abbreviations: ATGL, adipose triglyceride lipase; C, cancer; FA, fatty acid; HE, hematoxylin-eosin; 5hmC, 5-hydroxymethylcytosine; N, noncancerous tissue; PNPLA2, patatin like phospholipase domain containing 2; TG, triglyceride.

activation level. Knockdown or pharmacological inhibition of ATGL/PNPLA2 increased lipid accumulation and decreased cell proliferation in *KDM6B-KO* cells. ATGL/PNPLA2 overexpression facilitates the growth of cancer cells, including HCC cells^[43,48]. In NASH-related HCC, KDM6B loss may promote cell survival through activating ATGL (Figure 6C).

KDM6B expression patterns differ between cancer types, with downregulation in pancreatic and colon cancers but upregulation in prostate, kidney, gastric

ovarian, and lung cancers, indicating that KDM6B functional roles are highly cell type-specific and pathologic context-dependent^[49]. KDM6B expression is high in HCC with distant metastasis and has stem cell-like properties^[32]. In our study, the high KDM6B expression group had viral infection and high alpha-fetoprotein levels (Table 1). In contrast, low KDM6B expression was correlated with NAFLD-related HCC and high metabolic risk factors, such as obesity and hypertension. Thus, the biological characteristics and mechanisms of low and high

TABLE 1 Relationship between KDM6B expression and clinicopathological factors

Clinicopathological factor	KDM6B expression		p
	High (n = 62)	Low (n = 25)	
Sex			0.901
Male	43	17	
Female	19	8	
Age (mean ± SD) (y)	69 ± 11	69 ± 8	1.000
HBV	18	2	0.035 ^a
HCV	21	3	0.038 ^a
NBNC	23	20	<0.001 ^a
NAFLD	9	20	<0.001 ^a
NASH	7	19	<0.001 ^a
Obesity	17	18	<0.001 ^a
Hypertension	28	20	0.003 ^a
Diabetes	21	9	0.553
Dyslipidemia	10	7	0.206
Child-Pugh A/B	58/4	25/0	0.190
Plt (<10×10 ⁴)	10	2	0.320
PT (<80%)	14	9	0.199
Alb (<3.5 g/dL)	8	4	0.705
AST (>40 IU/L)	25	9	0.708
ALT (>40 IU/L)	20	9	0.738
Tbil (>1.0 mg/dL)	8	6	0.212
ICG-15 (>15%)	24	14	0.140
AFP (>20 ng/mL)	31	4	0.003 ^a
PIVKA-II (>40 mAU/mL)	35	12	0.474
Tumor size (>5 cm)	23	5	0.122
Tumor number (>2)	11	9	0.067
Differentiation (well, moderate/poor)	45/10	24/1	0.089

^aStatistical significance.

Abbreviations: Alb, albumin; ALT, alanine aminotransferase; AFP, alpha-fetoprotein; AST, aspartate aminotransferase; ICG-15, indocyanine green retention rate at 15 minutes; NBNC, nonhepatitis B and nonhepatitis C viral; PIVKA-II, protein induced by vitamin K absence II; Plt, platelet; PT, prothrombin time; Tbil, total bilirubin.

expressions of KDM6B in HCC carcinogenesis are distinct. Notably, KDM6B expression levels in primary HCC tissues were correlated with G0S2 expression levels, particularly in NAFLD-related HCC. These data indicate that KDM6B/G0S2-double low expression could be used as a biomarker for NAFLD-related HCC with resistance to lipotoxicity.

Understanding cancer metabolism, especially lipid metabolism, is critical for elucidating the mechanism of cancer development and progression and establishing new therapeutic strategies^[50]. Our data suggest that KDM6B-deficient HCC cells confer resistance to lipotoxicity via epigenetic downregulation of G0S2 expression and subsequent ATGL/PNPLA2 activation.

TABLE 2 Relationship between G0S2 and KDM6B expression and clinicopathological factors

Clinicopathological factor	G0S2 and KDM6B		p
	High (n = 47)	Low (n = 11)	
Sex			0.880
Male	31	7	
Female	16	4	
Age (mean ± SD) (y)	70 ± 10	68 ± 8	1.000
HBV	12	1	0.239
HCV	17	1	0.080
NBNC	18	9	0.020 ^a
NAFLD	9	9	<0.001 ^a
NASH	6	9	<0.001 ^a
Obesity	13	9	0.001 ^a
Hypertension	23	8	0.154
Diabetes	17	5	0.568
Dyslipidemia	9	4	0.218
Child-Pugh A/B	34/13	8/3	0.979
Plt (<10×10 ⁴)	10	1	0.353
PT (<80%)	12	5	0.191
Alb (<3.5 g/dL)	8	2	0.920
AST (>40 IU/L)	16	4	0.880
ALT (>40 IU/L)	13	3	0.980
Tbil (>1.0 mg/dL)	8	1	0.513
ICG-15 (>15%)	20	4	0.708
AFP (>20 ng/mL)	20	3	0.351
PIVKA-II (>40 mAU/mL)	29	9	0.206
Tumor size (>5 cm)	23	1	0.016 ^a
Tumor number (>2)	8	6	0.009 ^a
Differentiation	39/8	11/0	0.140

^aStatistical significance.

Abbreviations: Alb, albumin; ALT, alanine aminotransferase; AFP, alpha-fetoprotein; AST, aspartate aminotransferase; ICG-15, indocyanine green retention rate at 15 minutes; NBNC, nonhepatitis B and nonhepatitis C viral; PIVKA-II, protein induced by vitamin K absence II; Plt, platelet; PT, prothrombin time; Tbil, total bilirubin.

Therefore, targeting the KDM6B-G0S2-ATGL/PNPLA2 pathway may be a novel therapeutic strategy for NAFLD-related HCC.

DATA AVAILABILITY STATEMENT

The microarray data are available to the public using the specific Gene Expression Omnibus accession number (GSE211848). The other data available are within the article or its Supplemental Materials (<http://links.lww.com/HC9/A541>).

ACKNOWLEDGMENTS

The authors thank Hiromi Nagasaki and Dr. Norimichi Chiyonobu for their technical and clerical assistance.

They also thank Editage (www.editage.com) for English language editing.

FUNDING INFORMATION

This work was supported by Grants-in-Aid for Scientific Research (A; 19H01055 and B; 20H03526, 23H02979), Challenging Research (Exploratory; 20K21627), and Young Scientists (23K15388) from the Ministry of Education, Culture, Sports, Science and Technology of Japan; Research Grant from the Princess Takamatsu Cancer Research Fund; and P-CREATE (JP19cm0106540) and Program for Basic and Clinical Research on Hepatitis (JP21fk0210090, JP22fk0210102, and JP22fk0210106) from AMED (Japan Agency for Medical Research and Development).

CONFLICTS OF INTEREST

The authors have no conflicts to report.

ORCID

Yoshimitsu Akiyama  <https://orcid.org/0000-0003-2329-8041>

Shu Shimada  <https://orcid.org/0000-0002-4962-0636>

Shinji Tanaka  <https://orcid.org/0000-0002-7718-3453>

REFERENCES

- Febbraio MA, Reibe S, Shalpour S, Ooi GJ, Watt MJ, Karin M. Preclinical models for studying NASH-driven HCC: How useful are they? *Cell Metab.* 2019;29:18–26.
- Huang DQ, El-Serag HB, Loomba R. Global epidemiology of NAFLD-related HCC: Trends, predictions, risk factors and prevention. *Nat Rev Gastroenterol Hepatol.* 2021;18:223–38.
- Calle E, Rodriguez C, Walker-Thurmond KTM. Overweight, obesity, and mortality from cancer in a prospectively studied cohort of US adults. *N Engl J Med.* 2003;348:1625–38.
- Massoud O, Charlton M. Nonalcoholic fatty liver disease/nonalcoholic steatohepatitis and hepatocellular carcinoma. *Clin Liver Dis.* 2018;22:201–11.
- Oda K, Uto H, Mawatari S, Ido A. Clinical features of hepatocellular carcinoma associated with nonalcoholic fatty liver disease: A review of human studies. *Clin J Gastroenterol.* 2015;8:1–9.
- Nagaoki Y, Hyogo H, Ando Y, Kosaka Y, Uchikawa S, Nishida Y, et al. Increasing incidence of non-HBV- and non-HCV-related hepatocellular carcinoma: Single-institution 20-year study. *BMC Gastroenterol.* 2021;21:1–10.
- Farrell G, Schattenberg JM, Leclercq I, Yeh MM, Goldin R, Teoh N, et al. Mouse models of nonalcoholic steatohepatitis: Toward optimization of their relevance to human nonalcoholic steatohepatitis. *Hepatology.* 2019;69:2241–57.
- Itoh M, Suganami T, Nakagawa N, Tanaka M, Yamamoto Y, Kamei Y, et al. Melanocortin 4 receptor-deficient mice as a novel mouse model of nonalcoholic steatohepatitis. *Am J Pathol.* 2011;179:2454–63.
- Chiyonobu N, Shimada S, Akiyama Y, Mogushi K, Itoh M, Akahoshi K, et al. Fatty acid binding protein 4 (FABP4) overexpression in intratumoral hepatic stellate cells within hepatocellular carcinoma with metabolic risk factors. *Am J Pathol.* 2018;188:1213–24.
- Hyun J, Jung Y. DNA methylation in nonalcoholic fatty liver disease. *Int J Mol Sci.* 2020;21:8138.
- Lee J, Kim Y, Friso S, Choi SW. Epigenetics in non-alcoholic fatty liver disease. *Mol Aspects Med.* 2017;54:78–88.
- Lyall MJ, Thomson JP, Cartier J, Ottaviano R, Kendall TJ, Meehan RR, et al. Non-alcoholic fatty liver disease (NAFLD) is associated with dynamic changes in DNA hydroxymethylation. *Epigenetics.* 2020;15:61–71.
- Lee S, Woo DC, Kang J, Ra M, Kim KH, Lee SR, et al. The role of the histone methyltransferase EZH2 in liver inflammation and fibrosis in STAM NASH mice. *Biology (Basel).* 2020;9:93.
- Shen Y, Guo X, Wang Y, Qiu W, Chang Y, Zhang A, et al. Expression and significance of histone H3K27 demethylases in renal cell carcinoma. *BMC Cancer.* 2012;12:470.
- Park D, Hong S, Salinas R, Liu S, Sun S, Sgualdino J, et al. Activation of neuronal gene expression by the JMJD3 demethylase is required for postnatal and adult brain neurogenesis. *Cell Rep.* 2014;8:1290–9.
- Seok S, Kim YC, Byun S, Choi S, Xiao Z, Iwamori N, et al. Fasting-induced JMJD3 histone demethylase epigenetically activates mitochondrial fatty acid β -oxidation. *J Clin Invest.* 2018;128:3144–59.
- Ichioka M, Suganami T, Tsuda N, Shirakawa I, Hirata Y, Satoh-Asahara N, et al. Increased expression of macrophage-inducible C-type lectin in adipose tissue of obese mice and humans. *Diabetes.* 2011;60:819–26.
- Mayer N, Schweiger M, Romauch M, Grabner GF, Eichmann TO, Fuchs E, et al. Development of small-molecule inhibitors targeting adipose triglyceride lipase. *Nat Chem Biol.* 2013;9:785–7.
- Nechin J, Tunstall E, Raymond N, Hamagami N, Pathmanabhan C, Forestier S, et al. Hemimethylation of CpG dyads is characteristic of secondary DMRs associated with imprinted loci and correlates with 5-hydroxymethylcytosine at paternally methylated sequences. *Epigenetics Chromatin.* 2019;12:64.
- Oba A, Shimada S, Akiyama Y, Nishikawaji T, Mogushi K, Ito H, et al. ARID2 modulates DNA damage response in human hepatocellular carcinoma cells. *J Hepatol.* 2017;66:942–51.
- Liebisch G, Ahrends R, Arita M, Arita M, Bowden J, Ejsing C, et al. Lipidomics needs more standardization. *Nat Metab.* 2019;1:745–7.
- Hatano M, Migita T, Ohishi T, Shima Y, Ogawa Y, Morohashi KI, et al. SF-1 deficiency causes lipid accumulation in Leydig cells via suppression of STAR and CYP11A1. *Endocrine.* 2016;54:484–96.
- Subramanian A, Tamayo P, Mootha V, Mukherjee S, Ebert B, Gillette M, et al. Gene set enrichment analysis: A knowledge-based approach for interpreting genome-wide expression profiles. *Proc Natl Acad Sci USA.* 2005;102:15545–50.
- Yamamoto K, Tateishi K, Kudo Y, Sato T, Yamamoto S, Miyabayashi K, et al. Loss of histone demethylase KDM6B enhances aggressiveness of pancreatic cancer through downregulation of C/EBP α . *Carcinogenesis.* 2014;35:2404–14.
- Xu X, Feng L, Liu Y, Zhou WX, Ma YC, Fei GJ, et al. Differential gene expression profiling of gastric intraepithelial neoplasia and early-stage adenocarcinoma. *World J Gastroenterol.* 2014;20:17883–93.
- Montibus B, Cercy J, Bouschet T, Charras A, Maupetit-Méhouas S, Nury D, et al. TET3 controls the expression of the H3K27me3 demethylase Kdm6b during neural commitment. *Cell Mol Life Sci.* 2020;78:757–68.
- Zhao NQ, Li XY, Wang L, Feng ZL, Li XF, Wen YF, et al. Palmitate induces fat accumulation by activating C/EBP β -mediated G0S2 expression in HepG2 cells. *World J Gastroenterol.* 2017;23:7705–15.
- Asakawa M, Itoh M, Suganami T, Sakai T, Kanai S, Shirakawa I, et al. Upregulation of cancer-associated gene expression in activated fibroblasts in a mouse model of non-alcoholic steatohepatitis. *Sci Rep.* 2019;9:19601.

29. Myoung SH, Sun YP, Shinzawa K, Kim S, Kun WC, Lee JH, et al. Lysophosphatidylcholine as a death effector in the lipoapoptosis of hepatocytes. *J Lipid Res.* 2008;49:84–97.
30. Yang X, Lu X, Lombès M, Rha GB, Chi YI, Guerin TM, et al. The G0/G1 switch gene 2 regulates adipose lipolysis through association with adipose triglyceride lipase. *Cell Metab.* 2010;11:194–205.
31. Heckmann BL, Zhang X, Saarinen AM, Liu J. Regulation of G0/G1 switch gene 2 (G0S2) protein ubiquitination and stability by triglyceride accumulation and ATGL interaction. *PLoS One.* 2016;11:e0156742.
32. Sherry-Lynes MM, Sengupta S, Kulkarni S, Cochran BH. Regulation of the JMJD3 (KDM6B) histone demethylase in glioblastoma stem cells by STAT3. *PLoS One.* 2017;12:e0174775.
33. Tang Y, Zhang L, Tu T, Li Y, Murray D, Tu Q, et al. MicroRNA-99a is a novel regulator of KDM6B-mediated osteogenic differentiation of BMSCs. *J Cell Mol Med.* 2018;22:2162–76.
34. Udali S, Guarini P, Moruzzi S, Ruzzenente A, Tammen SA, Guglielmi A, et al. Global DNA methylation and hydroxymethylation differ in hepatocellular carcinoma and cholangiocarcinoma and relate to survival rate. *Hepatology.* 2015;62:496–504.
35. Zhao F, Ke J, Pan W, Pan H, Shen M. Synergistic effects of ISL1 and KDM6B on non-alcoholic fatty liver disease through the regulation of SNAI1. *Mol Med.* 2022;28:12.
36. Byun S, Seok S, Kim YC, Zhang Y, Yau P, Iwamori N, et al. Fasting-induced FGF21 signaling activates hepatic autophagy and lipid degradation via JMJD3 histone demethylase. *Nat Commun.* 2020;11:807.
37. Heckmann BL, Zhang X, Xie X, Liu J. The G0/G1 switch gene 2 (G0S2): Regulating metabolism and beyond. *Biochim Biophys Acta.* 2013;1831:276–81.
38. Wang Y, Zhang Y, Qian H, Lu J, Zhang Z, Min X, et al. The G0/G1 Switch gene 2 is an important regulator of hepatic triglyceride metabolism. *PLoS One.* 2013;8:e72315.
39. El-Assaad W, El-Kouhen K, Mohammad AH, Yang J, Morita M, Gamache I, et al. Deletion of the gene encoding G0/G1 switch protein 2 (G0S2) alleviates high-fat-diet-induced weight gain and insulin resistance and promotes browning of white adipose tissue in mice. *Diabetologia.* 2015;58:149–57.
40. Yan S, Yang XF, Liu HL, Fu N, Ouyang Y, Qing K. Long-chain acyl-CoA synthetase in fatty acid metabolism involved in liver and other diseases: An update. *World J Gastroenterol.* 2015;21:3492–8.
41. Li T, Li X, Meng H, Chen L, Meng F. Acs1 affects triglyceride levels through the ppar γ pathway. *Int J Med Sci.* 2020;17:720–7.
42. Ellis JM, Li LO, Wu P-C, Koves TR, Ilkayeva O, Stevens RD, et al. Adipose acyl-CoA synthetase-1 (ACSL1) directs fatty acids towards β -oxidation and is required for cold thermogenesis. *Cell Metab.* 2010;12:53–64.
43. Zhang R, Meng J, Yang S, Liu W, Shi L, Zeng J, et al. Recent advances on the role of ATGL in cancer. *Front Oncol.* 2022;12:1–12.
44. Romeo S, Savage DB. Lipase tug of war: PNPLA3 sequesters ABHD5 from ATGL. *Nat Metab.* 2019;1:505–6.
45. Romeo S, Kozlitina J, Xing C, Pertsemlidis A, Cox D, Pennacchio LA, et al. Genetic variation in PNPLA3 confers susceptibility to nonalcoholic fatty liver disease. *Nat Genet.* 2008;40:1461–5.
46. Wang Y, Kory N, BasuRay S, Cohen JC, Hobbs HH. PNPLA3, CGI-58, and inhibition of hepatic triglyceride hydrolysis in mice. *Hepatology.* 2019;69:2427–41.
47. Huang Y, He S, Li JZ, Seo YK, Osborne TF, Cohen JC, et al. A feed-forward loop amplifies nutritional regulation of PNPLA3. *Proc Natl Acad Sci USA.* 2010;107:7892–7.
48. Liu M, Yu X, Lin L, Deng J, Wang K, Xia Y, et al. ATGL promotes the proliferation of hepatocellular carcinoma cells via the p-AKT signaling pathway. *J Biochem Mol Toxicol.* 2019;33:e22391.
49. Zhang X, Liu L, Yuan X, Wei Y, Wei X. JMJD3 in the regulation of human diseases. *Protein Cell.* 2019;10:864–82.
50. Cheng C, Geng F, Cheng X, Guo D. Lipid metabolism reprogramming and its potential targets in cancer. *Cancer Commun (Lond).* 2018;38:27.

How to cite this article: Hatano M, Akiyama Y, Shimada S, Yagi K, Akahoshi K, Itoh M, et al. Loss of KDM6B epigenetically confers resistance to lipotoxicity in nonalcoholic fatty liver disease-related HCC. *Hepatol Commun.* 2023;7:e0277. <https://doi.org/10.1097/HC9.0000000000000277>